

RIGID ROTATION AND THE KERR METRIC

Gerald E. Marsh

Argonne National Laboratory (Ret)
5433 East View Park
Chicago, IL 60615

E-mail: gemarsh@uchicago.edu

Abstract. The Einstein field equations have no known and acceptable interior solution that can be matched to an exterior Kerr field. In particular, there are no interior solutions that could represent objects like the Earth or other rigidly rotating astronomical bodies. It is shown here that there exist closed surfaces upon which the frame-dragging angular velocity and the red-shift factor for the Kerr metric are constant. These surfaces could serve as a boundary between rigidly rotating sources for the Kerr metric and the Kerr external field.

PACS: 04.20.Jb, 04.70.Bw

Key Words: Rigid Rotation; Kerr Metric

Introduction.

The Kerr solution to the Einstein field equations is generally thought to be the only possible stationary, axially symmetric and asymptotically flat solution that could represent the gravitational field outside an uncharged rotating body. It is characterized by two parameters, the angular momentum per unit mass a , and the mass m , and is often discussed in Boyer-Lindquist coordinates,¹ which will also be used here

The uniqueness of the Kerr solution does not mean that it plays the role of a Birkhoff theorem for rotating massive objects. What is the case is that the space-time geometry outside a rotating mass asymptotically approaches that of the Kerr solution. The reason for this is that the multipole moments of the Kerr solution are closely related while those of real mass distributions may in principle be independently specified. Because higher multipole fields fall off rapidly with distance from the source, the gravitational field of a rotating object will asymptotically approach that of the Kerr solution. There is then a contradiction between the uniqueness theorems for the Kerr solution and the near external field of real rotating masses.

An approximation to the gravitational potential due to the multipoles of the Kerr solution² is given by $(-1)^{n+1} m (a^{2n}/r^{2n+1}) P_{2n}(\cos\theta)$. A real astronomical body undergoing gravitational collapse would have to selectively radiate away some of its multipole moments so as to satisfy this relation if the Kerr solution were to represent the end state of its exterior gravitational field. As put by Thorne³ many years ago, “Because of this relationship between multipole moments and angular momentum, the Kerr solution cannot represent correctly the external field of *any* realistic stars (except for a <<set of measure zero>>).”

The other problem with the Kerr solution is that it has no known acceptable interior solution. That is, one that is non-singular and able to be matched to the exterior solution on the boundary; i.e., the metric tensor g_{ij} and its first order partial derivatives should be continuous across the boundary.

Interior Solutions.

Because of the polar (or zenith) angle dependent frame-dragging effect inherent in the Kerr solution (also known as the Lense-Thirring effect), one generally considers some form of rotating fluid for the interior solution so as to be able to satisfy the boundary conditions, generally on an oblate spheroidal coordinate surface corresponding to $r = \text{constant}$ in Boyer-Lindquist coordinates. Since the paper by Hernandez², a large literature on perfect fluid interior solutions for the Kerr metric has appeared. Krasinski⁴ has given a careful review of the various approaches to this problem.

Burghardt⁵ has recently given an exact interior metric that represents a differentially rotating fluid and which successfully matches the exterior Kerr metric. It also reduces to the Schwarzschild interior solution when the rotational parameter is set equal to zero. Because the Burghardt metric illustrates the complexity and difficulty finding possible Kerr interior solutions, it is worth examining in a little more detail.

The Burghardt metric, converted to Boyer-Lindquist coordinates,⁶ is given by

$$ds^2 = \left(1 - \frac{r^2}{R^2}\right)^{-1} \left(1 - \frac{a^2 \sin^2 \theta}{a^2 + r^2}\right) dr^2 + (r^2 + a^2 \cos^2 \theta) d\theta^2 + \left(1 - \frac{a^2 \sin^2 \theta}{a^2 + r^2}\right)^{-1} \left((a^2 + r^2)^{1/2} \sin \theta d\phi - \frac{a \sin \theta}{(a^2 + r^2)^{1/2}} dt \right)^2 - a_T^2 \left(1 - \frac{a^2 \sin^2 \theta}{a^2 + r^2}\right)^{-1} (dt - a^2 \sin^2 \theta d\phi)^2, \quad (1)$$

where

$$a_T = \frac{1}{2} \left[\left(1 + 2 \left(\frac{r_g^2 + a^2}{r_g^2 - a^2} \right) \right) \left(1 - \frac{r_g^2}{R^2} \right)^{1/2} - \left(1 - \frac{r^2}{R^2} \right)^{1/2} \left(\frac{r_g^2 - a^2}{r_g^2 + a^2} \right) \right], \quad (2)$$

and

$$R = (r_g^2 + a^2)^{1/2} \left(\frac{r_g}{2m} \right)^{1/2}. \quad (3)$$

Here, $r \leq r_g$ and the subscript g indicates the value of the variable at the boundary surface.

For $a = 0$, the metric becomes

$$ds^2 = \left(1 - \frac{2mr^2}{r_g^3}\right)^{-1} dr^2 + r^2 d\theta^2 + r^2 \sin^2 \theta d\phi^2 - \frac{1}{4} \left[3 \left(1 - \frac{2m}{r_g}\right)^{1/2} - \left(1 - \frac{2mr^2}{r_g^3}\right)^{1/2} \right]^2 dt^2, \quad (4)$$

which is the constant density Schwarzschild interior solution. Note that this solution does not have a singularity at $r = 0$ like the vacuum Schwarzschild solution.

After setting $r = r_g$ in the Burghardt metric, the angular velocity of the frame-dragging effect reduces—after some algebra—to that of the Kerr exterior solution,

$$\omega = -\frac{g_{t\phi}}{g_{\phi\phi}} = \frac{2amr}{(r^2 + a^2)^2 - a^2(a^2 - 2mr + r^2)\sin^2 \theta}. \quad (5)$$

Thus, the Burghardt interior metric will indeed match the θ -dependent frame-dragging rotation of the Kerr solution across the boundary. Conceptually, one may interpret ω as the angular velocity at any point along the trajectory of a falling particle, initially released far from the source of the field with zero angular momentum with respect to the rotation axis, as viewed from a reference frame at infinity.

As noted by Burghardt, this interior metric is singular for $r = 0$ and $\theta = \pi/2$ where the vacuum Kerr metric is also singular. If one computes the Einstein tensor for this metric,⁷ it too is singular for these coordinates. This does not occur with the interior Schwarzschild solution, which does not retain the singularity of the vacuum solution.

Surfaces of constant red-shift factor and frame-dragging velocity

Thorne's comment quoted above about the multipole moments of the Kerr solution does not rule out the existence of all interior solutions but only relegates the class of such solutions to “a set of measure zero” in the context of gravitational collapse. The introduction of surfaces of constant red-shift and frame-dragging velocity would simplify

the problem of matching the Kerr exterior field to rotating solid bodies. The possibility of doing this was foreshadowed by Thorne.

In discussing the Kerr solution with regard to rotating objects, one generally considers only cases where $m > a$. But it should be noted, at least in passing, that most common rotating objects, like the Earth or a rotating 33 rpm record,⁸ have parameters where $a \gg m$. For the vacuum Kerr solution this means the singularity is not hidden behind a horizon, but this would not be a problem for real rotating objects since the Kerr exterior solution would apply only outside the boundary of the interior solution for the object, and the interior solution would not be acceptable if it were singular.

If it is indeed possible to use a rigidly rotating solid body as the interior solution for the Kerr field, it is necessary that the differential rotation of the bounding surface vanish. For this to be the case, there are a number of conditions that must be satisfied:

- I. The exterior Kerr solution must have a closed surface such that on it the frame-dragging angular velocity is constant; i.e., independent of the Boyer-Lindquist θ coordinate.
- II. That surface, if it exists, must also have a constant angular velocity as measured relative to a reference frame at infinity.
- III. The red-shift factor, defined below, must also be a constant on the surface for photons emitted with zero angular momentum relative to the rotation axis.³

It will now be shown that it is possible to satisfy these three conditions, and that such surfaces do exist and can be found analytically.

The red-shift factor is defined as

$$\left(u^t\right)^{-2} = g_{tt} + 2g_{t\phi}\Omega + g_{\phi\phi}\Omega^2, \quad (6)$$

where u^t is the time component of the 4-velocity and $\Omega = \frac{u^\phi}{u^t} = \frac{d\phi}{dt}$ is the angular velocity as measured relative to a reference frame at infinity.

For a rigidly rotating body, the surface has no differential rotation so that Ω must be a constant. To match the Kerr exterior field, we also need to have ω constant so that there is no differential frame dragging at the boundary of the body. If we set these constants equal, we have $K = \omega = \Omega$. The red-shift factor then becomes

$$(u^t)^{-2} = g_{tt} - g_{t\phi}K. \quad (7)$$

For the Kerr solution one has

$$g_{tt} = \frac{r^2 - 2mr + a^2 \cos^2 \theta}{r^2 + a^2 \cos^2 \theta}, \quad g_{t\phi} = 4 \frac{mra \sin^2 \theta}{r^2 + a^2 \cos^2 \theta}, \quad (8)$$

so that the red-shift factor becomes

$$(u^t)^{-2} = \frac{r^2 - 2mr + a^2 \cos^2 \theta - 4Kma \sin^2 \theta}{r^2 + a^2 \cos^2 \theta}. \quad (9)$$

Since this must be constant on the surface of the rigidly rotating body, we look for solutions to the equation

$$\frac{r^2 - 2mr + a^2 \cos^2 \theta - 4Kma \sin^2 \theta}{r^2 + a^2 \cos^2 \theta} - C = 0, \quad (10)$$

where C is another constant not equal to K . This equation is soluble and yields the solutions

$$r_1 = - \frac{m + 2Kma \sin^2 \theta + \frac{1}{2} \left(-4a^2(C-1)^2 \cos^2 \theta + 4(m + 2Kma \sin^2 \theta)^2 \right)^{1/2}}{C-1},$$

$$r_2 = - \frac{m + 2Kma \sin^2 \theta - \frac{1}{2} \left(-4a^2(C-1)^2 \cos^2 \theta + 4(m + 2Kma \sin^2 \theta)^2 \right)^{1/2}}{C-1}. \quad (11)$$

The parameters and the range of θ must be such that

$$\left(-4a^2(C-1)^2 \cos^2 \theta + 4(m + 2Kma \sin^2 \theta)^2 \right)^{1/2} \quad (12)$$

is real. Note that r_1 and r_2 are invariant under the combination of $a \rightarrow -a$ and $K \rightarrow -K$. Such a transformation corresponds to a reversal of the direction of rotation.

The meaning of the constant C , which sets the value of constant red shift factor, can be understood by a comparison with the Newtonian potential, where $g_{tt} = 1 - 2U$, $g_{t\phi} = 0$, and $g_{\phi\phi} = -r^2 \sin^2 \theta$. Thus,

$$(u')^{-2} = 1 - 2U - r^2 \Omega^2 \sin^2 \theta. \quad (13)$$

Here U is the total Newtonian surface potential—with the positive sign convention, where $U > 0$. C effectively controls the “radius” of the constant red-shift and frame-dragging surface. Radius is put in quotes since because the surface is not in general spherical.

Since $(u')^{-2}$ is a constant, rearranging the terms in Eq. (13) gives $U + \frac{1}{2}r^2\Omega^2 \sin^2 \theta = \text{Constant}$. This says that the total potential at the surface of a non-deformable rotating spherical body is constant. The second term on the left might be called the “centrifugal potential”. In general, for a deformable or fluid body, the total potential U includes the gravitational potential resulting from the change in radius at the surface due to the deformation as well as the potential due to the change in mass distribution caused by the deformation—sometimes called the “self-potential”, both of which depend on θ .

The red-shift factor $(u')^{-2}$ should not be confused with the actual red shift from the surface of the body, which is given by $1/u'$. The distinction will be important in what follows.

In order to plot the solutions to Eqs. (11) in Cartesian coordinates one must convert the expressions given above in Boyer-Lindquist coordinates to Cartesian coordinates. The transformation from Boyer-Lindquist to Cartesian coordinates is

$$\begin{aligned}x &= \left(r^2 + a^2\right)^{1/2} \sin\theta_{B-L} \cos\phi \\y &= \left(r^2 + a^2\right)^{1/2} \sin\theta_{B-L} \sin\phi \\z &= r \cos\theta_{B-L}.\end{aligned}\tag{14}$$

For clarity, in the above equations and in what follows below, the subscripts $B-L$ and C have been added where needed to distinguish between Boyer-Lindquist and Cartesian variables. From Eq. (14), one readily shows that

$$\frac{x^2 + y^2}{r^2 + a^2} + \frac{z^2}{r^2} = 1.\tag{15}$$

The relationship between the coordinates is shown in Figure 1, drawn for $\phi = 0$.

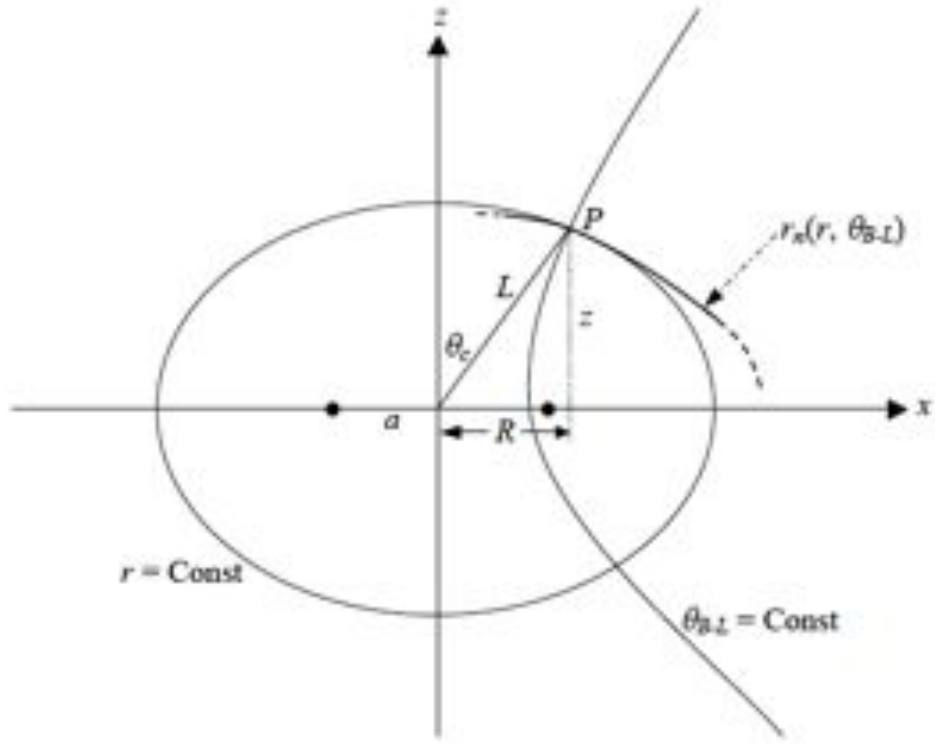


Figure 1. The figure shows a portion of the constant frame-dragging and red-shift surface given by $r_n(r, \theta_{B-L})$, where n corresponds to one of the two roots r_1 or r_2 of Eq.(11). The constant Boyer-Lindquist coordinate surfaces that intersect $r_n(r, \theta_{B-L})$ at the point $P \in r_n(r, \theta_{B-L})$ are designated by $r = \text{Const}$ and $\theta_{B-L} = \text{Const}$. θ_C is the Cartesian polar angle corresponding to the point P , which also has Cartesian coordinates z and x . The distance $R = (x^2 + y^2)^{1/2}$, and the figure is drawn for $y = 0$ corresponding to $\phi = 0$. The two dots at $x = \pm a$ correspond to the ring singularity at $r = 0$, $\theta_{B-L} = \pi/2$.

From the figure, we have

$$\begin{aligned} z &= L \cos \theta_C \\ R &= L \sin \theta_C. \end{aligned} \tag{16}$$

so that

$$\frac{L^2 \sin^2 \theta_C}{r^2 + a^2} + \frac{L^2 \cos^2 \theta_C}{r^2} = 1. \tag{17}$$

L is then given by

$$L = \left(\frac{r^2(r^2 + a^2)}{r^2 + a^2 \cos^2 \theta_C} \right)^{1/2}. \quad (18)$$

With $\phi = 0$, Eqs. (16) and (18) allow $r_n(r, \theta_{B-L})$ to be plotted in Cartesian coordinates. In doing so, however, the Boyer-Lindquist θ in r_n will be interpreted by the plotting program of Mathematica^{®9} as θ_C . It will be seen, however, that for the examples given below, the error is very small.

In order to plot the examples that follow, it is necessary to determine the value of the constant C . The red shift from a body of mass m and radius r , as measured far from the body, is given in mks units by $1/u^t = \sqrt{1 - \frac{2Gm}{c^2 r}}$. C is given by the square of this quantity. Three examples will be given, that of the Sun, the canonical neutron star (defined as having a radius of $10km$, a mass of 1.4 solar masses, and a period of $1.5ms$), and the Earth. The following table gives the value of $1/u^t$ for each of these cases.

	$1/u^t = \sqrt{1 - \frac{2Gm}{c^2 r}}$
SUN	0.999997878
NEUTRON STAR	0.765871
EARTH	0.9999999932

Table 1. The red shift $1/u^t$ for the Sun, the canonical neutron star, and the Earth. Note that $C = (1/u^t)^2$.

The plot of the constant red-shift and frame-dragging surface r_1 , for the Sun, is shown in Fig. 2. The oblateness is greatly exaggerated in the figure by the choice of aspect ratio; the actual eccentricity, given by

$$e = \sqrt{\frac{x^2 - z^2}{x^2}}, \quad (19)$$

is essentially zero.

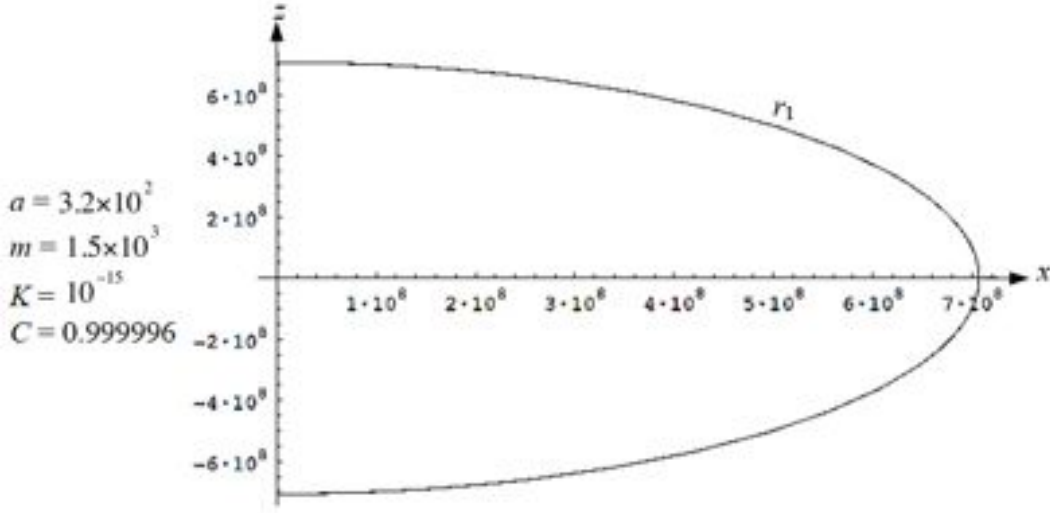


Figure 2. The constant red-shift and frame-dragging surface given by the first solution, r_1 , of Eq.(11) for parameters corresponding to the Sun. a , m and K are in geometrized units, while C is dimensionless. The oblateness of the surface is greatly exaggerated by the choice of aspect ratio. Because of the cylindrical symmetry, the full surface is obtained by rotating the figure around the z -axis.

For comparison, the radius of the Sun is $7 \times 10^8 m$, which is just slightly less than the radius of the constant red-shift and frame-dragging surface at $\theta = \pi/2$. The surface given by the second solution of Eq. (11), r_2 , does not give a physically acceptable surface. The plotting method used for Fig. 2 also has large errors when applied to r_2 . The same is the case for r_2 of the other examples given below.

For the parameters corresponding to the canonical neutron star, one obtains the plot shown in Fig. 3. The value of a is calculated from the neutron star angular momentum given by Dessart, et al.¹⁰ and K from the period.

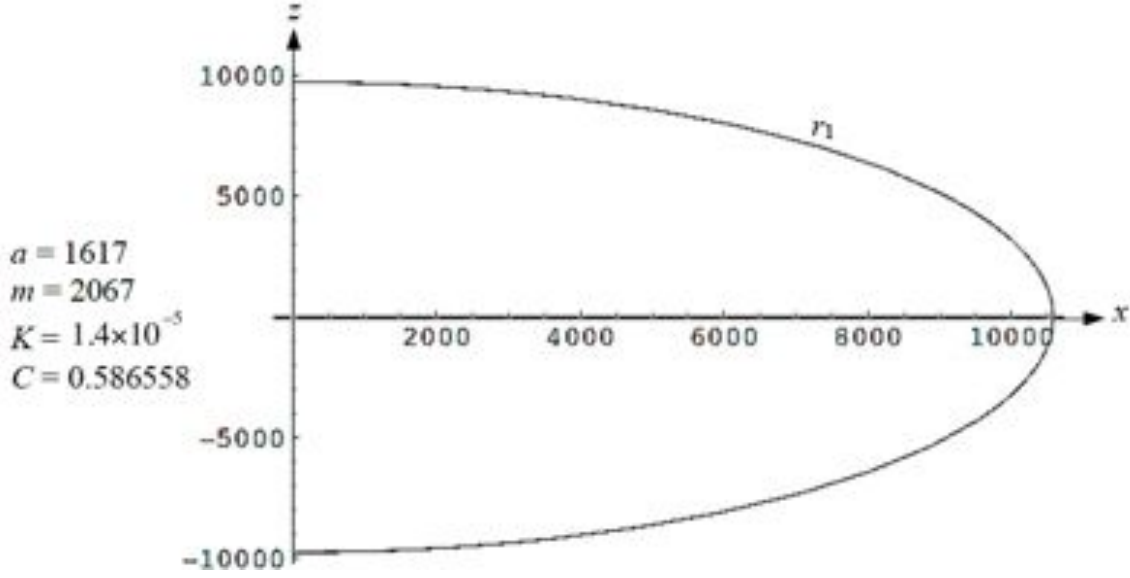


Figure 3. Canonical neutron star constant red-shift and frame-dragging surface given by the first solution, r_1 , of Eq.(11). a is calculated from the neutron star angular momentum given by Dessart, et al. and K from the period.

The eccentricity of the surface shown in Fig. 3 is $e = 0.15$. The oblateness ε , determined from $\varepsilon + 1 = (1 - e^2)^{-1/3}$, is 7.6×10^{-3} , close to the value of the Crab pulsar¹¹ where $\varepsilon \sim 10^{-3}$. As can be seen, at $\theta = \pi/2$ the radius of this surface is 1.06 times greater than the canonical neutron star radius of 10 km.

The final example is that of the Earth, for which there is also data from the Gravity Probe B experiment. The frame-dragging measurement gave a value of -37.2 ± 7.2 milliarc sec/yr or $\sim 6.4 \times 10^{-15}$ rad/sec. Converted to geometrical units, this is $\sim 2.1 \times 10^{-23} m^{-1}$. The surface is shown in Fig. 4.

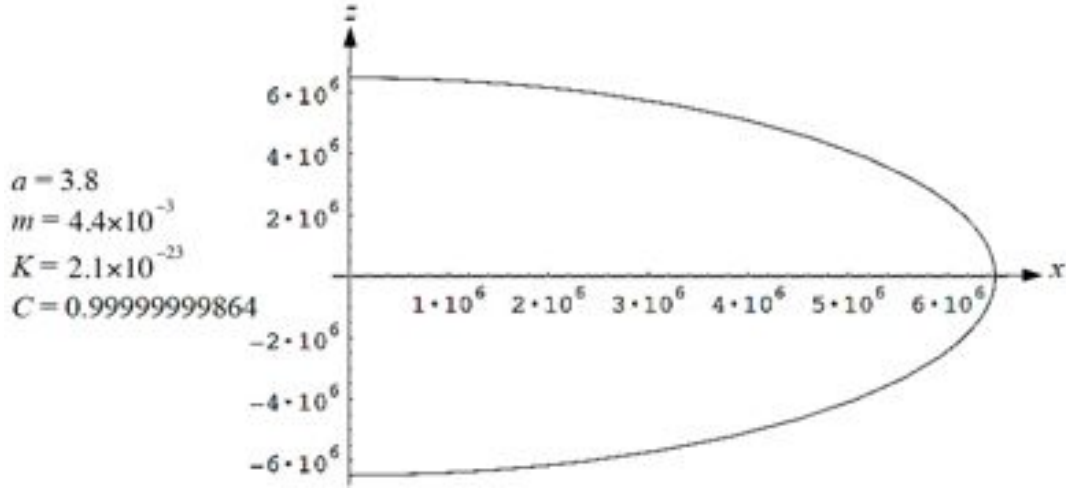


Figure 4. Constant red-shift and frame-dragging surface given by the first solution, r_1 , of Eq.(11) for the Earth. The constant K is set by the frame-dragging measurements of the Gravity probe B experiment. Note that for the Earth $a \gg m$.

Here the eccentricity is, as was the case for the Sun, essentially zero. Since the radius of the Earth is 6.4×10^6 m, at $\theta = \pi/2$ this surface, with radius $\sim 6.48 \times 10^6$, is only slightly larger than the radius of the Earth., and just a bit smaller than the Gravity Probe B orbital radius of $\sim 7 \times 10^6$.

The multipole issue

The magnitude of the multipole contribution to the potential at the location of the surfaces of constant red shift and frame dragging will now be shown to be very small compared to the Newtonian potential.

The approximate potential for the multipoles associated with the Kerr metric that was given by Hernandez, Jr. and discussed above can be written as

$$V = - \sum_{n=0}^{\infty} \frac{(-1)^n m a^{2n}}{r^{2n+1}} P_{2n}(\cos \theta) = -\frac{m}{r} - \sum_{n=1}^{\infty} \frac{(-1)^n m a^{2n}}{r^{2n+1}} P_{2n}(\cos \theta). \quad (20)$$

The first term on the right hand side of this equation is, of course, the Newtonian potential, while the second is the contribution of the multipoles.

The structure of this potential is not unique to the Kerr metric. It also appears when computing the Newtonian potential for an oblate spheroid¹², whose ellipticity is not too great, at points exterior to the spheroid. The above examples meet this criterion, and the potential can be shown to be

$$V_{Newtonian} = -\frac{m}{r} - \sum_{n=1}^{\infty} \frac{(-1)^n m a^{2n}}{(2n+1)(2n+3) r^{2n+1}} P_{2n}(\cos\theta). \quad (21)$$

In the Newtonian case, the multipole fields fall off faster because of the numerical factor $(2n+1)(2n+3)$ in the denominator.

For the examples above, Table 2 shows the contribution to the potential of the first 10 terms of the multipole expansion compared to that of the Newtonian potential. The nominal radius and ellipticity are also given for comparison purposes.

	Nominal Radius (m)	Ellipticity	m/z ($\theta = 0$)	m/x ($\theta = \pi/2$)	Multipole
SUN	7×10^8	~ 0	2.12×10^{-6}	2.12×10^{-6}	2.24×10^{-19}
NEUTRON STAR	10^4	0.15	0.212	0.195	5.71×10^{-3} ($\theta=0$)
					4.74×10^{-3} ($\theta=\pi/2$)
EARTH	6×10^6	~ 0	6.8×10^{-10}	6.8×10^{-10}	1.2×10^{-22}

Table 1. The relative contributions to the overall potential of the first ten terms of the multipole expansion compared to that of the Newtonian potential at the position of the constant red-shift and frame-dragging surface.

As can be seen, even in the case of the neutron star, the multipole contribution to the potential at the position of the constant red-shift and frame-dragging surface is very small compared to the Newtonian potential. For the neutron star, the only case for which there is a significant difference, the potential due to the multipoles is given for the z -axis at $\theta = 0$ and the x -axis at $\theta = \pi/2$.

Plotting errors

The plotting error for Figs. 2, 3, and 4 can be estimated from

$$\cos \theta_C - \cos \theta_{B-L} = \frac{z}{L} - \frac{z}{r} = \left(\frac{1}{L} - \frac{1}{r} \right) z = \left(\frac{1}{L} - \frac{1}{r} \right) L \cos \theta_C. \quad (22)$$

Plotting this expression for the neutron star, which has the largest error—the other examples having an error on the order of 10^{-14} , gives the result shown in Fig. 5.

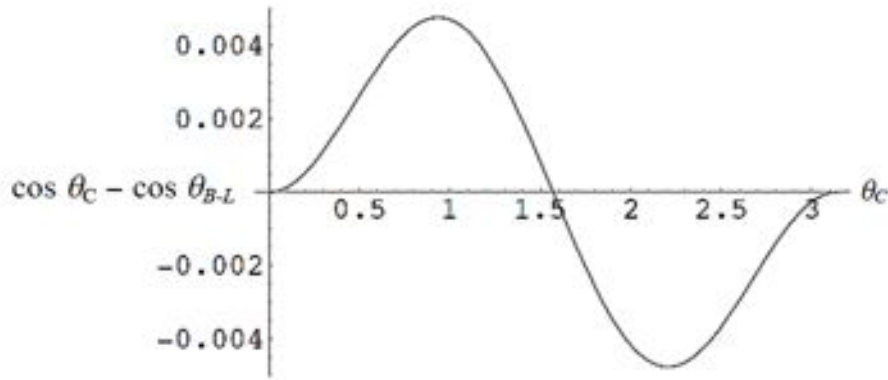


Figure 5. The plotting error introduced by the method of plotting used in the figures above is greatest for the case of the neutron star and is shown in this figure.

Note the plotting error is very small and vanishes for $\theta = 0, \pi/2$, and π .

Summary

The differential frame-dragging effect inherent in the Kerr metric generally restricts consideration to some form of rotating fluid for the interior solution so as to be able to satisfy the boundary conditions. However, it has been shown here that there exist surfaces of constant red-shift and frame-dragging angular velocity that could serve as the boundary between the exterior Kerr field and an interior solution for a rigidly rotating solid body. Examples of such surfaces were found for parameters corresponding to the Sun, the canonical neutron star, and the Earth. The results are at least consistent with actual data from neutron star modeling and the Gravity Probe B experiment.

REFERENCES

- ¹ R. H. Boyer and R. W. Lindquist, “Maximal Analytic Extension of the Kerr Metric”, *J. Math. Phys.* **8**, 265-281 (1967).
- ² W.C. Hernandez, Jr., “Material Sources for the Kerr Metric”, *Phys. Rev.* **159**, 1070-1072 (1967).
- ³ K.S. Thorne, “Relativistic Stars, Black Holes and Gravitational Waves (Including an in-Depth Review of the Theory of Rotating, Relativistic Stars), contained in B.K. Sachs, ed., *General Relativity and Cosmology*, Proceedings of the International School of Physics <<Enrico Fermi>> Course XLVII, pp. 237-283, Academic Press (1971).
- ⁴ A. Krasinski, “Ellipsoidal Space-Times, Sources for the Kerr Metric”, *Annals of Physics* **112**, 22-40 (1978).
- ⁵ R. Burghardt, “A Kerr Interior”, *Sitzungsberichte der Leibniz-Sozietät der Wissenschaften zu Berlin* **92**, 51–60 (2007).
- ⁶ Geometrical units are used; see, for example: R.M. Wald, *General Relativity*, Appendix F (University of Chicago Press, Chicago 1984). For convenience, the general connection between conventional and geometrical coordinates is as follows: If a quantity in *mks* units has the dimension $L^n T^m M^p$, where L , T , M , correspond to length, time, and mass respectively, then in geometrical units the dimension would be given by L^{n+m+p} . The conversion factor from *mks* to geometric units is $c^m (c^2/G)^p$, where c is the velocity of light and G is the gravitational constant.
- ⁷ The code used to find the Einstein tensor was the EinsteinTensor package written by Pekka Janhunen of the Finnish Meteorological Institute Geophysics Dept. Also useful was the EDCRGTCcode.m (<http://www.inp.demokritos.gr/~sbonano/RGTC/>).
- ⁸ C. Hoenselaers, “The Double Kerr Solution: A Survey”, *Proceedings of the Fourth Marcel Grossmann Meeting on General Relativity*, R. Ruffini (ed), pp. 967-975 (1986).
- ⁹ In Mathematica[®] one must also take into account that $\theta = 0$ corresponds to the x -axis while in B-L coordinates it is the z -axis.

¹⁰ L. Dessart, et al., “Multi-Dimensional Simulations of the Accretion-Induced Collapse of White Dwarfs to Neutron Stars”, *ApJ* **644**, 1063 (2006); (ArXiv:astro-phy0601603). (2006).

¹¹ S.L. Shapiro and S.A. Teukolsky, *Black Holes, White Dwarfs and Neutron Stars: The Physics of Compact Objects* (Wiley-VCH Verlag GmbH & Co. KGaA, Weinheim 2004).

¹² A.G. Webster, *The dynamics of particles and of rigid, elastic, and fluid bodies* (B.G. Teubner, Leipzig 1904), Ch. VIII, Art.161, p. 424.